Invasion percolation with memory

Hooshang Kharabaf and Yanis C. Yortsos
Department of Chemical Engineering, University of Southern California, Los Angeles, California 90089-1211
(Received 15 November 1996; revised manuscript received 30 January 1997)

Motivated by the problem of finding the minimum threshold path (MTP) in a lattice of elements with random thresholds τ_i, we propose a new class of invasion processes, in which the front advances by minimizing or maximizing the measure $S_n=\Sigma_i \tau_i^n$ for real n. This rule assigns long-time memory to the invasion process. If the rule minimizes S_n (case of minimum penalty), the fronts are stable and connected to invasion percolation in a gradient [J. P. Hulin, E. Clement, C. Baudet, J. F. Gouyet, and M. Rosso, Phys. Rev. Lett. **61**, 333 (1988)] but in a correlated lattice, with invasion percolation [D. Wilkinson and J. F. Willemsen, J. Phys. A **16**, 3365 (1983)] recovered in the limit $|n|=\infty$. For small n, the MTP is shown to be related to the optimal path of the directed polymer in random media (DPRM) problem [T. Halpin-Healy and Y.-C. Zhang, Phys. Rep. **254**, 215 (1995)]. In the large n limit, however, it reduces to the backbone of a mixed site-bond percolation cluster. The algorithm allows for various properties of the MTP and the DPRM to be studied. In the unstable case (case of maximum gain), the front is a self-avoiding random walk. [S1063-651X(97)08805-3]

PACS number(s): 47.55.Mh, 64.60.Ak, 05.40.+j

I. INTRODUCTION

Many processes of practical interest involve disordered media or lattices of elements with randomly distributed thresholds $\tau_i>0$. The typical problem consists of the application of an overall difference in potential (or in pressure in the case of fluid flow in porous media), $\Delta\Phi$, across opposite ends of a lattice (or of the pore network representing the porous medium). A lattice element remains closed to transport if the local potential difference is smaller than its threshold $\Delta\phi_i<\tau_i$, but becomes open in the opposite case $\Delta\phi_i>\tau_i$. In these problems, a quantity of significant interest is the minimum overall threshold, $\Delta\Phi_{\min}$, or, equivalently, the minimum gradient

$$|\nabla\Phi|_{\min}(L)\equiv\frac{\Sigma_i\tau_i}{L} \tag{1}$$

at which a path of open elements first forms. In the above, the sum is over the minimum threshold path (MTP), which is unknown and must also be determined. The problem typically arises in networks of diodes [1], in the flow of Bingham plastics in porous media [2], and in the mobilization of foams in porous media [3]. In a more general context, where each threshold is viewed as a penalty [3], it is a problem of determining the minimum overall penalty (a problem in global optimization).

Roux *et al.* [1] studied aspects of this problem in the context of a network of diodes, by considering two different cases, one in which the path is directed (no backtracking allowed) and one in which it is not. They suggested that $|\nabla\Phi|_{\min}$ is akin to a percolation threshold and studied its dependence on the lattice size L. Their findings showed finite-size scaling similar to directed percolation (DP) or ordinary percolation (OP), respectively, from which they concluded that the onset of connectivity in this problem is of the same universality class as percolation. Using numerical simulations in two-dimensional (2D) lattices of thresholds uniformly distributed in (0,1), they further estimated $|\nabla\Phi|_{\min}(\infty)=0.231$ and $|\nabla\Phi|_{\min}(\infty)=0.227$ for the directed and nondirected cases, respectively. They also made the very interesting observation that the two problems of the onset of conduction in a lattice of thresholds and percolation, ought to be connected, as their respective thresholds are special cases of the more general expression

$$\mathcal{L}_n=\min\left(\frac{\Sigma_i\tau_i^n}{L}\right)^{1/n} \tag{2}$$

with $n=1$ corresponding to the threshold-lattice problem and $|n|=\infty$ to OP. Additional information on the MTP or on its connection to percolation, was not provided, however.

Sahimi [2] provided estimates of $|\nabla\Phi|_{\min}(\infty)$ and conjectured that the MTP has the same scaling properties as the well-studied minimum path $l_{\min}$ of a percolation cluster. The latter (also known as the chemical distance) denotes the path on the percolation cluster with the minimum total length (or tortuosity). It is known to be a self-similar fractal [4], scaling as $l\sim L^{D_{\min}}$, where $D_{\min}$ is equal to 1.13 in 2D and 1.34 in 3D. Rossen and Mamun [3] proceeded along similar lines and proposed a percolation approach for the MTP, consisting of occupying lattice elements with progressively higher thresholds. Although commenting that such a process is actually only an approximation, they also identified the MTP with the minimum path $l_{\min}$ of the percolation cluster thus obtained.

Closely related to the above is the problem of a directed polymer in random media (DPRM) (see [5] and references therein). Here, a well-studied version involves a directed (stretched) polymer in a square lattice with one end anchored at the origin ($x=0$, $y=0$), which is allowed to move in discrete steps along the two directions x and y, subject to the

constraint $|y(x+1)-y(x)|=0$ or 1, and that the polymer cannot turn back in the x direction (overhangs not allowed). An energy cost ϵ randomly distributed, is associated with every step. The objective is to find the configuration that minimizes the total energy. This problem was mapped to the celebrated Kardar-Parisi-Zhang (KPZ) equation (see [6]), which is known to give rise to self-affine fractals, and is also connected to the more general problem of interface growth and surface roughening (for example, wetting in porous media, burning of paper, etc.) which also lead to self-affine fractals. As the MTP and DPRM problems both involve the minimization of a global quantity, we expect that they also would be closely related.

At present, a firm connection of the lattice-threshold problem to percolation appears to be lacking. In particular, the relation of the MTP to the minimum path of percolation, if it indeed exists, is not self-evident. The latter pertains to the minimum sum of equal length segments on the OP cluster, while the former is the minimum sum of distributed thresholds in a regular lattice. Understanding this connection forms the main objective of this paper. We present a new algorithm for the construction of the MTP, based on which its properties can be studied. The novelty of the algorithm is that it requires the simulation of an invasion process, similar to invasion percolation (IP), except that here the rules for the front advance depend on the front history, as explained below. In implementing this algorithm, and in conjuction with the remark in Ref. [1], however, we realized that the MTP problem can benefit from the study of more general invasion processes, in which the front advances by minimizing (or maximizing) the general measure

$$S_n=\sum_i \tau_i^n \tag{3}$$

for n real, and where the sum is over any path connecting any site at the front to the inlet boundary. As these involve the entire history of the process, we will refer to them as invasion percolation with memory (IPM). Both the nondirected and the directed problems are considered.

In the nondirected case, the properties of invasion and of the generalized MTP, over which S_n is minimal, are studied. It is shown that the process of minimizing S_n is related to invasion percolation in a gradient (IPG) [7], but in a correlated lattice, from which it is inferred that the invasion fronts are rough, but not self-similar at all scales. A connection of the MTP to the backbone of a mixed site-bond percolation cluster (obtained in the limit $|n|=\infty$) is, next, established. In the directed case, the IPM algorithm allows for a generalization of the DPRM problem to arbitrary values of n and shows that the optimal path of the latter approaches the backbone of the mixed site-bond directed percolation cluster. We note in advance that an important difference between our approach and the conventional one is that here we identify the optimum configuration between any two curves (namely, the polymer can originate from any point on a given curve, and not from the origin only). For $n=1$, the optimum path in the DPRM problem and the MTP are found to be very similar, although not identical, based on which we conjecture that the MTP in the small n limit is also self-affine. The identification (opening) of paths of higher energy, as the applied potential difference exceeds the minimum value, is briefly studied. Finally, for the sake of generalization, we also consider the case of maximizing S_n (maximum gain), where, in the presence of a trapping rule, the front is shown to be a self-avoiding random walk (SAW).

Before we proceed, we note that the consideration of the various moments of τ is equivalent to considering distributions of new thresholds $\eta=\tau^n$, with probability density function (PDF), arithmetic mean and standard deviation equal to

$$f(\eta)=\frac{1}{|n|}\,\eta^{(1/n)-1},\quad \langle\eta\rangle=\frac{1}{n+1},\quad \sigma_\eta=\frac{n}{(1+n)\sqrt{1+2n}}, \tag{4}$$

respectively. For the more general problem of finding the MTP of arbitrary threshold distributions, we expect a rough analogy between patterns with the same ratio of standard deviation to arithmetic mean $m\equiv\sigma_\eta/\langle\eta\rangle$, which for the present case reads $m=n/\sqrt{1+2n}$. Thus, we anticipate that the results for large or small n would be analogous to those for processes with arbitrary threshold distributions and large or small m, respectively. From Eq. (4), it is apparent that for the existence of the arithmetic mean we must have $n>-1$, while for that of the variance, $n>-1/2$. Therefore, for finite first and second moments of general threshold distributions, we must restrict Eq. (3) to $n>-1/2$. However, some results for smaller n (which formally correspond to Levy flights [8]) will also be presented (see Kharabaf [9] for more details). We note that the DPRM problem with the PDF of Eq. (4) and n in the range $(-1/2,0)$ was singled out as a special case by Marconi and Zhang [8] who found that, in that range, the meandering growth exponent varies with n.

The paper is organized as follows. First, the basic rules of the algorithm and the construction of the MTP are presented. The process is generalized to arbitrary n and it is shown that it reduces to IP in the two limits $n\to\pm\infty$. Then we discuss the application of the same algorithm to the solution of a simple version of the DPRM problem. IPM is subsequently shown to be related to IPG in a correlated lattice, where an appropriate Bond number is defined. Based on this analogy, the properties of the invasion fronts are elucidated. From these two relations to DPRM and IPG, it is suggested that the invasion fronts and the corresponding MTPs of IPM are generally rough, reducing to self-similar fractals only in the limit $|n|=\infty$. Various properties of the fronts and the MTP are studied. Then, the properties of higher-energy paths as the applied potential difference increases above its minimum value, are briefly discussed. Finally, we present an extension of the IPM process to the destabilizing case, where S_n is maximized and where the front is shown to reduce to a SAW.

II. IPM PROCESSES

Invasion algorithm

Consider an invasion process from right to left in a lattice of sites and bonds. Invader and defender reside on the sites of the lattice. The bonds have thresholds τ_i, randomly assigned from a uniform distribution in (0,1). The invading front advances one site at a time following rules to be de-

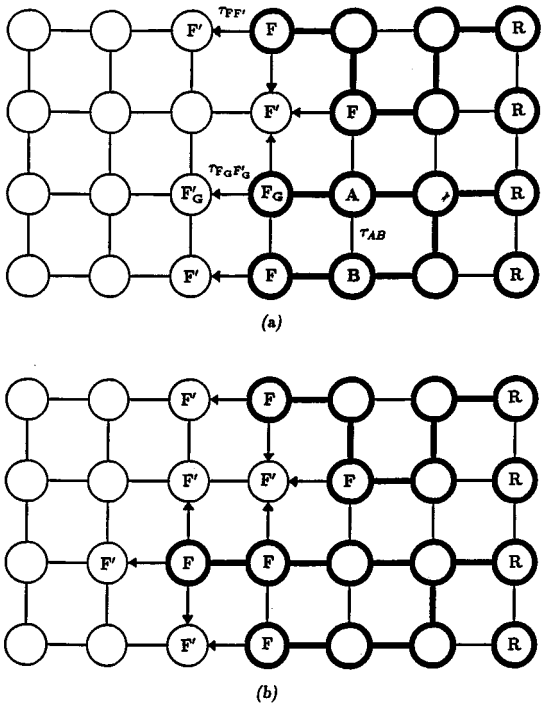

FIG. 1. Description of the invasion rules, before (a) and after (b) a growth step. Invasion occurs from right to left. F denotes a front site, F' a perimeter site, F_G is a growth site and F'_G is the site occupied next. The process is site-occupancy bond-invasion percolation.

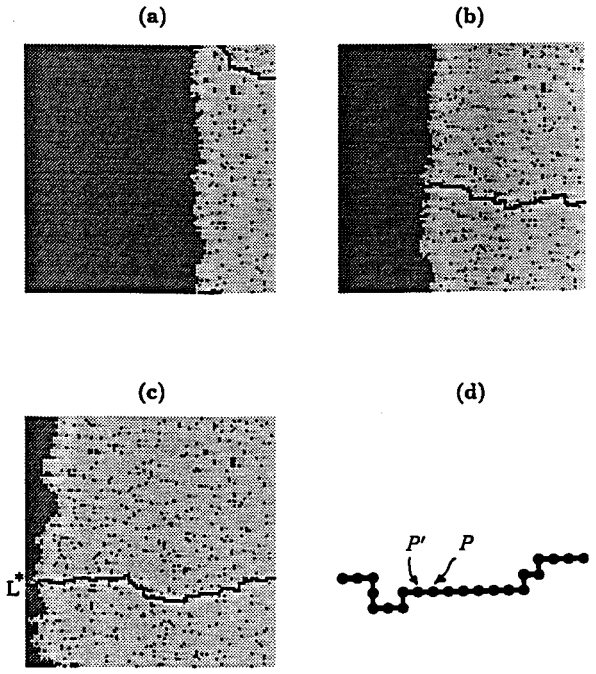

FIG. 2. Snapshots of the invasion process (occupied sites in gray) and of the MTP at different stages of invasion (a)–(c) for $n=1$ in a 100×100 square lattice. Periodic boundary conditions were used. L^* denotes the site at ''front breakthrough'' on the left boundary. (d) shows the terminology used to identify the MTP. Note that the MTP at different stages is not necessarily a subset of the final MTP.

scribed below. Because both sites and bonds are involved, this problem is actually a mixed site-bond problem, which is prototypical of fluid displacements in porous media [10]. The rule for the front advance is as follows: Denote by F an arbitrary site currently on the front, by F' one of its (nearest-neighbor) perimeter sites in the defender region [Fig. 1(a)] (where a 2D square lattice is used), by F_G the site from which invasion will actually proceed next, and by F'_G the perimeter site to which the front advances during the next step [Fig. 1(b)]. A value $V_n(F)$ is recursively assigned to every site F on the front (hence, to all sites that have been invaded), through the following algorithm.

Let $\tau_{FF'}$ denote the threshold connecting site F with one of its perimeter sites F', and form the sum

$$S_{n,FF'}=V_n(F)+\tau^n_{FF'}. \tag{5}$$

Then, the threshold to be invaded next will connect the two sites, a ''growth'' site F_G and the site to be occupied next, F'_G, for which $S_{n,FF'}$ is minimum. We point out that in our terminology, the term growth site has a different meaning from that of Roux and Guyon [11]. Having made this determination, site F_G is identified, the front advances to F'_G, the assignment

$$V_n(F'_G)=V_n(F_G)+\tau^n_{F_GF'_G} \tag{6}$$

is subsequently made and the process is repeated. In this way, and by using the initial condition $V_1(R)=0$ for all sites R on the initial interface (which here is the right boundary, but could be any other curve) (Fig. 1), all invaded sites are assigned a unique value V_n. In contrast to IP, where the front advances by the local rule of selecting the smallest (or largest) available threshold, here the advance depends on the past history, thus imparting to the process a long-time memory. Through this algorithm, it is straightforward to show that the value $V_n(A)$, assigned to every invaded site A, actually represents the minimum sum of thresholds among all paths that connect A to the right boundary (see Appendix A). The corresponding minimum path from A to the injection (initial) side can be easily identified, as discussed below.

Typical snapshots of the occupied sites and of the corresponding MTP for $n=1$ in a 2D square lattice are shown in Fig. 2 at different stages of invasion [Figs. 2(a)–2(c)]. Both the front and the MTP have the appearance of rough but not self-similar curves. The MTP across the lattice can be directly identified when the front first reaches the left-hand side (LHS) boundary [at ''breakthrough,'' site L^*, Fig. 2(c)]. It can be traced recursively, by starting from L^*, proceeding in the direction of decreasing V_n and identifying the next site P that belongs to the path, and neighbors a site P' already on this path [Fig. 2(d)], by requiring that the condition $V_n(P')=V_n(P)+\tau^n_{PP'}$, be identically satisfied. A similar procedure is used to find the minimum paths (from the current front location to the right boudary) during the different stages of invasion [Figs. 2(a)–2(b)], as well as the MTP originating from any invaded site A. These paths are not necessarily subsets of the MTP.

In the simulations shown in Fig. 2, a trapping rule similar

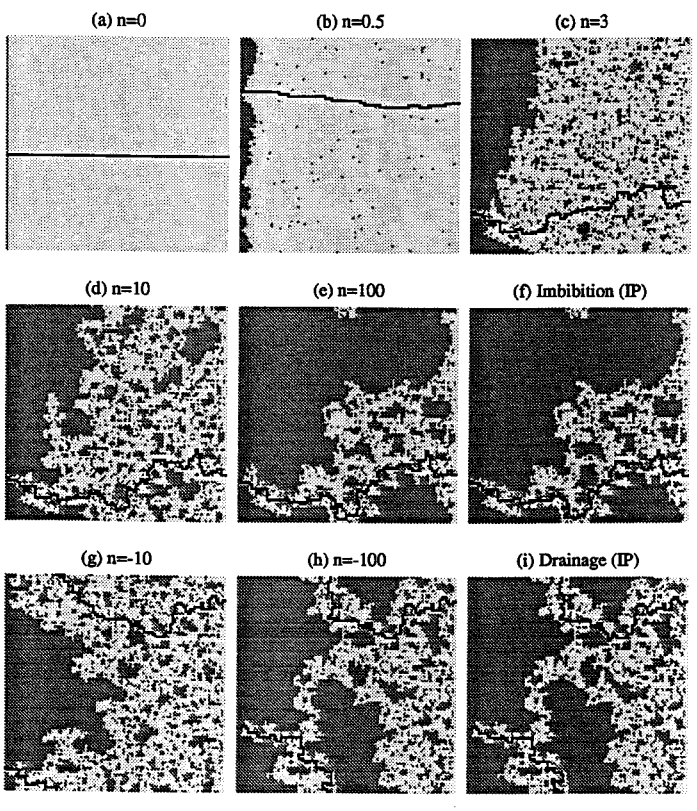

FIG. 3. Invasion fronts at ''breakthrough'' and corresponding MTPs in a 100×100 lattice, for $n=0$ (a), $n=0.5$ (b), $n=3$ (c), $n=10$ (d), $n=100$ (e). Pattern (f) is invasion percolation, where the front advances by penetrating the bond with the smallest threshold. Pattern (g) is for $n=-10$, pattern (h) for $n=-100$, and pattern (i) corresponds to invasion percolation, where the front advances by penetrating the bond with the largest threshold. Note the similarity of (e) with (f) and of (h) with (i). Fronts become more self-similar, and the fraction of trapped sites increases (MTPs are more tortuous) as n increases.

to invasion fercolation with trapping (IPT) [12] was applied, such that a trapped site cannot be invaded. Thus, in the invaded region, there exist closed regions, the sites of which have not been visited (Fig. 2). However, this does not affect the values of V_n or the minimum path, as any paths that traverse trapped regions cannot, by construction, be minimum paths. In the cases shown in Fig. 2, the number density of the trapped regions is high, although their size is small. We must point out, however, that by relaxing the trapping rule, and by continuing the invasion process following breakthrough, all sites of the lattice can be invaded.

Because the function V_1 is taken to be single valued, a site cannot be invaded more than once, hence a noninvaded bond between two adjacent sites at the front, such as F and F_G in Fig. 1, cannot become open in any subsequent step (it is trapped). This has the following consequences: (i) Between any invaded site A and the right boundary there is one and only one self-avoiding path occupied by invaded sites. By construction (see Appendix A), this path is the MTP from A to the boundary. (ii) Because of this absence of reconnections, all invaded sites belong to distinct dendritic branches which originate from the right boundary, but, otherwise, do not intersect one another (see also below). (iii) Depending on the coordination number Z of the lattice, an occupied site can be the growth site for two or more branches, but cannot be the termination point of two branches.

The IPM algorithm bears some relation with the ''burning trees'' algorithm of Herrmann *et al.* [13] for obtaining information on the backbone and other properties of the percolation cluster, and to the matrix transfer algorithm used in the DPRM problem. In the former, a process mimicking invasion in a percolation cluster is considered and invaded sites are labelled sequentially using consecutively increasing integers. However, the IPM algorithm is more general. The ''burning trees'' algorithm results as a special case of the IPM problem if the invasion is restricted to a percolation cluster only, all thresholds take the same value, and a standard invasion percolation rule is taken for the invading front. The matrix transfer algorithm can also be obtained as a special case of IPM if the invasion is initiated from a single point only. We also mention an alternative but rather cumbersome algorithm, also employed in MTP, which involves solving the Laplace equation in the original lattice, using an applied potential difference sufficiently large for all elements to be open to conduction and incrementally reducing the potential until flow ceases, at which point the minimum pressure gradient is identified [2].

Patterns

Typical patterns of the invasion fronts at breakthrough, along with the corresponding generalized MTP, are shown in Fig. 3 for various values of n. In these and subsequent simulations, lattice sizes ranged from 50×50 to 500×500 in 2D, and from $10\times10\times10$ to $40\times40\times40$ in 3D.

At small values of $|n|$, the fronts appear to be self-affine, with front widths and trapped fraction of sites decreasing with decreasing $|n|$. For $n=0$ [Fig. 3(a)], the displacement is compact, the front width is equal to the pixel size, there are no trapped sites, and the MTP is a straight line, as the minimum measure S_0 is simply the smallest Euclidean distance from the front to the right boundary. At a slightly larger n [Fig. 3(b)] the MTP appears to have the structure of a multifaceted curve. As n increases further [Figs. 3(d)–3(e)], front width and trapped fractions increase, and the MTP is more tortuous. In the limit $n\to\infty$, the patterns are shown to

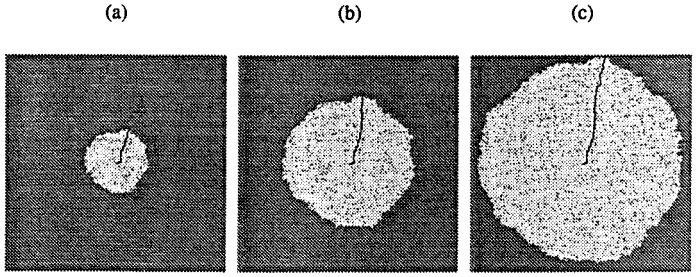

FIG. 4. Invasion pattern and the corresponding MTP for $n=1$ for IPM in radial geometry (originating from a single point).

approach IP [Fig. 3(f)], where the front advances by selecting the perimeter site with the minimum size. The corresponding IP pattern [Fig. 3(f)] suggests that this is indeed the case. The same also holds for the case $n\rightarrow-\infty$ [compare Fig. 3(h) and Fig. 3(i)], where it can be shown that the pattern approaches that of IP, where the front advances by invading the bond with the maximum size [9].

To prove the reduction to the IP problem in the limit $n\rightarrow\infty$, we proceed as follows. Consider any two pairs of neighboring sites (F_1,F_1') and (F_2,F_2') such that the threshold of the bond F_1F_1' is smaller than that of bond F_2F_2'

$$\tau_{F_1F_1'}<\tau_{F_2F_2'}. \tag{7}$$

We will show that in the large n limit the following inequality holds

$$V_n(F_1)+\tau^n_{F_1F_1'}<V_n(F_2)+\tau^n_{F_2F_2'}. \tag{8}$$

If valid, this implies that site F_1' is invaded before site F_2', which is the desired IP rule. For the proof, we rearrange Eq. (8) to read

$$V_n(F_1)<V_n(F_2)+\tau^n_{F_2F_2'}\left[1-\left(\frac{\tau_{F_1F_1'}}{\tau_{F_2F_2'}}\right)^n\right] \tag{9}$$

and take the large n limit. In view of Eq. (7), the inequality in this limit further reduces to

$$V_n(F_1)<V_n(F_2)+\tau^n_{F_2F_2'}. \tag{10}$$

However, the latter is always valid, as its reverse implies $V_n(F_2')<V_n(F_1)$, namely, that site F_2' has been occupied before site F_1, in contradiction with our implied assumption that site F_2' is a perimeter site. It follows that in this limit, it is the bond with the smallest threshold that is invaded next. This is identical to the IP rule (which in this particular example has a rough physical analog in imbibition, namely, the displacement of a wetting by a nonwetting fluid in porous media [10]). An identical argument applies for the limit $n\rightarrow-\infty$, except that now it is the bond with the largest threshold that is occupied next [9]. Either problem involves site occupancy, bond percolation with bond trapping. The existence of bond trapping is important for the properties of the limiting percolation problems. Patterns in the range $(-1/2,0)$ were also investigated, in view of the special attention paid to this range in the corresponding DPRM problem. The patterns were found to be similar to the case of small and positive n, however.

The IPM algorithm can readily simulate IPM in a radial geometry, in which invasion originates from a single point. In essence, this is a modification of the conventional DPRM problem to invasion which is not directed. An invasion pattern and the corresponding MTP for $n=1$ is shown in Fig. 4. The pattern reveals a rather compact displacement with a rough front, quite analogous to the rectilinear invasion case. Similar results were found for the same process in 3D lattices [9]. Finally, we note that processes with other measures can also be defined: For example, we may consider a *stage* process, where each element (stage) has efficiency τ_i, with $0<\tau_i<1$, and where the maximization of the overall efficiency $\Pi_i\tau_i$, is sought. Through the transformation $\eta=-\ln\tau$, the problem can be mapped into the case $n=1$, considered previously, except that now the measure to be minimized is $H=-\Sigma_i\ln\tau_i$, namely, the thresholds are distributed in the different interval $(0,\infty)$. Likewise, we may define the information (entropy) measure $I=-\Sigma_i\tau_i\ln\tau_i$. The minimization of either H or I also leads to fronts similar to the $n=1$ case (see [10]).

Directed invasion

The IPM algorithm was next modified to simulate a directed invasion percolation process. In this version, the front is not allowed to invade bonds in a direction opposite to the main invasion direction (which in the illustrations of Fig. 1–3 is from right to left). As a result, the corresponding MTP is also directed. To show this, we recall that the tracing of the MTP involves the successive connection of pairs of sites, which at some stage of the process were a front growth site and its perimeter site to be occupied next, respectively. As a result, this renders the MTP directed. Using arguments identical to Appendix A for the nondirected case we can show that the directed version leads to the identification of paths that are directed and also minimize the sum of thresholds. In particular, the MTP at breakthrough corresponds to the optimal path of the simplest version of the DPRM problem which shares the same origin as the MTP. The IPM algorithm can be used in the study of more general DPRM problems, and we hope to report on these in the future.

Snapshots of the resulting patterns are shown in Fig. 5 for various values of n. In the case $n=1$, the optimal path of the DPRM problem is known to be a self-affine curve with a zero transverse average, but with an increasing variance

$$\langle|y(x)|\rangle\sim x^{\nu_{DP}}, \tag{11}$$

where the meandering exponent ν_{DP} has the exact value $\nu_{DP}=2/3$ [14]. As pointed out, this problem can be mapped to the KPZ equation [6], which is a generic model for surface

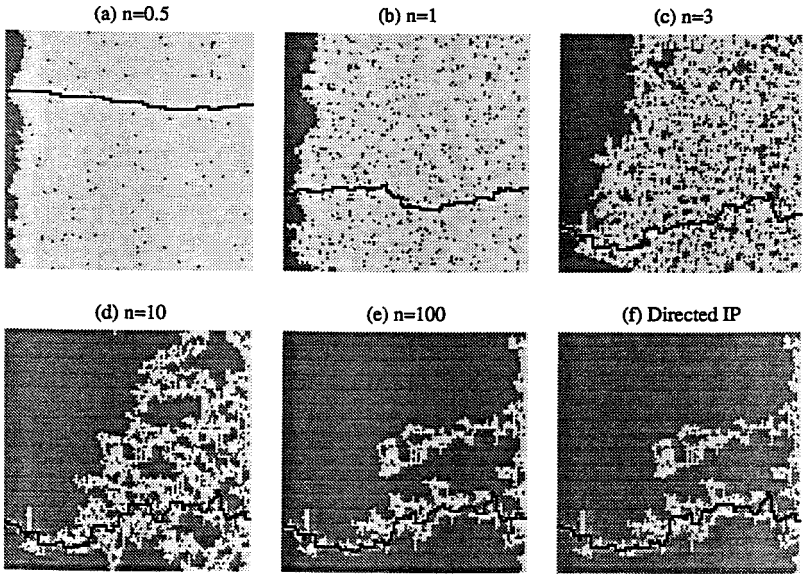

FIG. 5. Invasion fronts at ''breakthrough'' and corresponding MTPs for directed invasion and for $n=0.5$ (a), $n=1$ (b), $n=3$ (c), $n=10$ (d), $n=100$ (e), and directed IP (f). The optimal path of this DPRM at large n is the backbone of a directed percolation cluster.

roughening and surface growth. The self-affine behavior is apparent in Fig. 5(b). As in the nondirected case, the path appears to be multifaceted for sufficiently small n [Fig. 5(a)], while fronts and minimum paths become more tortuous as n increases [Figs. 5(c)–5(d)]. In the limit $|n|\to\infty$ the problem becomes a directed, site-occupancy bond IP with bond trapping, and the optimal path becomes its backbone [see Fig. 5(e) and Fig. 5(f)]. The approach to this limit can also be proved theoretically using arguments similar to those for the nondirected case. The significant variation of the path properties as n varies has not been reported previously, to our knowledge, most investigations having focused on either $n=1$ or $-1/2<n<0$. In fact, the apparent effect of disorder in varying the patterns from multifaceted (at small n) to self-similar (at $n\to\infty$) is analogous to the behavior reported in [15], in a different context, and deserves further attention, as it may contradict the apparent universality associated with the DPRM problem.

Comparison with the nondirected case (Fig. 3) shows that for small values of n the two processes are identical (for example, compare the patterns for $n=1$ or smaller, and also note the very close similarity even for $n=3$). In fact, the two patterns for $n=1$ in Figs. 3 and 5 are identical, although this happens to be a coincidence of the particular realization. Different realizations show that the MTP for $n=1$ contains occasional overhangs, the probability of which is briefly discussed below. As n increases to larger values the difference between directed and nondirected invasion increases, both with respect to the invasion patterns and the resulting MTP. The close relation between nondirected and directed IPM processes at small n suggests that the MTP for $n=1$ has properties similar to the optimal path of the DPRM. On the other hand, the divergence of patterns and paths at larger n shows that this connection does not extend to arbitrary threshold distributions, and specifically those involving relatively large n (large threshold variance or large m). We infer that the MTP coincides with the optimal path of the DPRM at small n, but it differs from it at larger n.

III. CONNECTION TO GRADIENT PERCOLATION

In essence, the IPM algorithm simulates an invasion percolation process, in which the front advances by penetrating perimeter sites with the smallest value of V_n. The front dynamics reflect the distribution of this field, and to understand better the IPM process, it is necessary to consider the distribution of V_n. For future use, we need to point out that the value of V_n at a site can be likened to the energy of the minimum path from that site to the boundary, just as in the DPRM problem, the statistics of which have been well elucidated.

Figure 6 shows various properties of the distribution of V_1 for a fixed spatial location x (namely, over all sites on a column transverse to the main invasion direction). The PDFs at a fixed x appear to be close to a Gaussian [Fig. 6], but with spatially varying arithmetic mean $\overline{V_1}$, and standard deviation σ_{V_1}, and to have the general dependence

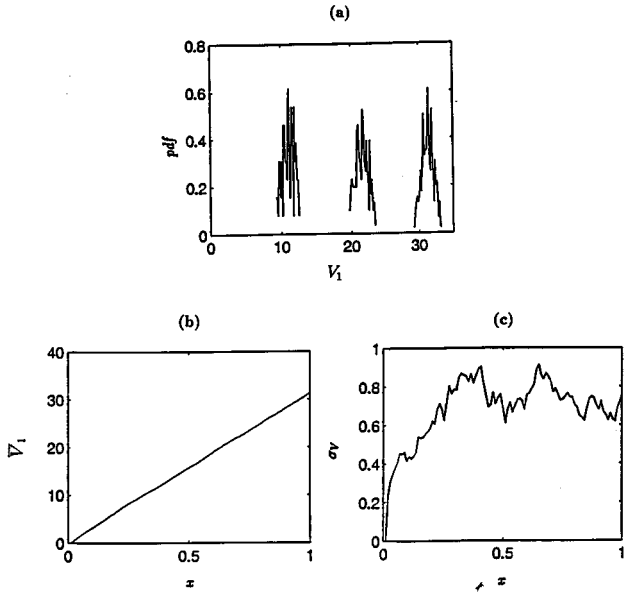

FIG. 6. Statistics of the energy (cost) distribution V_1 from simulations in a 100×100 lattice: (a) The PDF at three different values of x (equal to 0.25, 0.50, and 0.75), (b) the variation of the arithmetic mean $\overline{V_1}$ with x, and (c) the variation of the standard deviation, σV_1 with x.

$$f(V,x)=\frac{g(\zeta)}{\sigma_{V_1}(x)}. \tag{12}$$

Here g is the distribution function, the precise form of which is not important to this paper, and we have defined the normalized variable $\zeta=[V-V(x)]/[\sigma_{V_1}(x)]$. The functional form (12) is consistent with the corresponding results for the DPRM problem [16]. The variation of V_1 with x is shown in Fig. 6(b). After a short transient, the mean is found to increase linearly with distance, with a constant slope C_1, which is closely related to $\mathcal{L}_1$. The latter also varies with distance, to reflect the finite-size scaling anticipated from [1]. Analogous results are expected for the general n case, where we have $dV_n/dx\rightarrow C_n$. However, we expect that the approach to the limit is much slower at large n, and, in fact, that at $n\rightarrow\infty$ the transient lasts until breakthrough. The variation of the mean with distance is consistent with the corresponding result in the DPRM problem, where [16]

$$\frac{d\langle E\rangle}{dx}=D_1+D_2x^{-(2/3)}. \tag{13}$$

The variation of the standard deviation, σ_{V_1}, is shown in Fig. 6(c). It is apparent that the variance increases (at least for a substantial fraction of the lattice length), although its rate of increase diminishes at larger x, suggesting a power-law variation with an exponent smaller than unity. We recall [16] that the corresponding DPRM problem has the scaling

$$\sigma_E\sim L^{1/2}f\left(\frac{x}{L^{(3/2)}}\right), \tag{14}$$

where L is the lattice size and the function f has the asymptotic behavior, $f\sim x^{1/3}$ for $x\ll 1$ and $f\sim$const for $x\gg 1$. By analogy, therefore, we expect a similar scaling for the general n MTP problem

$$\sigma_{V_n}\sim L^{\chi_n}f_n\left(\frac{x}{L^{z_n}}\right), \tag{15}$$

where the exponents χ_n and z_n may depend on n and need to be determined. This is not attempted here. In this paper, we will proceed only with the assumption that $0<\chi_n<1$, as suggested in the simulations. In passing, we note that previously reported DPRM simulations pertain to $n=1$, and it is possible that the exponents of Eqs. (13) and (14) may also vary as a function of n. This problem also deserves further attention.

From the above it is apparent that V_n consists of a transverse average linearly increasing with x and of a perturbation, ψ, namely,

$$V_n=C_nx+\psi, \tag{16}$$

with $\overline{\psi}=0$ and with σ_ψ scaling as in Eq. (15). In view of the previous, the ratio of the standard deviation to the mean must decrease as x increases. The two facts that the transverse average of V_n increases with x and that the rule for the front advance is to seek the minimum V_n, suggests that IPM is closely related to IPG. We recall that IPG is invasion percolation in an externally applied gradient (e.g., due to a body force, such as gravity, or to a gradient in the bond size [17]), giving rise to a percolation probability gradient measured by the Bond number B. The invasion pattern has the fractal properties of an IP cluster near the front over a scale equal to the front width σ_F, but it occupies a compact region away from it. The front width scales with B as [7]

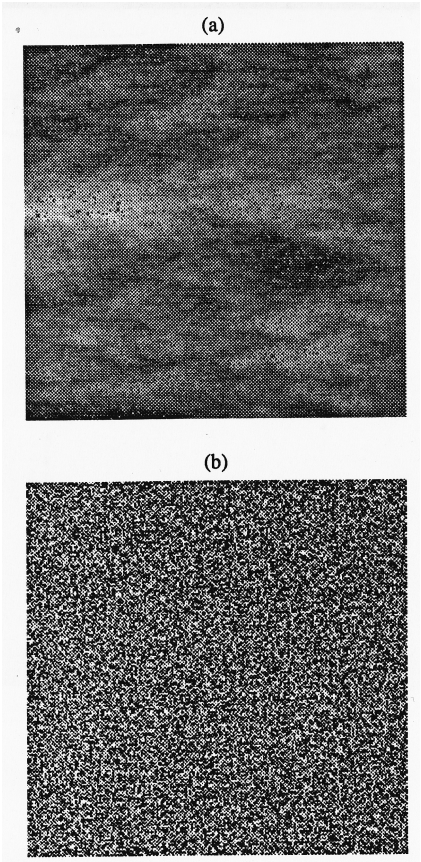

FIG. 7. Grayscale plot of the perturbation ψ for $n=1$ from simulations in a 200×200 lattice (a). (b) shows a Gaussian noise for the same lattice. Darker colors correspond to smaller values.

$$\sigma_F\sim B^{-[\nu/(\nu+1)]}, \tag{17}$$

where ν is the OP correlation length exponent.

To investigate the connection to IPG, the properties of the perturbation ψ are needed. Figure 7 shows a grayscale plot of ψ obtained from simulations in a 200×200 lattice. Also shown, for comparison, is a map of white noise on the same lattice [Fig. 7(b)]. It is clear that the noise generated by the IPM is not an uncorrelated white noise (as in standard IPG) but it is *correlated* in space. For a more quantitative measure of the correlation we constructed the variograms of ψ in the two different directions [9]. Both variograms displayed correlations growing as a power law in space, similar to fractional Brownian motion (fBm), with a positive Hurst exponent (H) [18]. For the case $n=1$, we found $H=0.32<0.5$ and $H=0.41<0.5$ in the respective directions. The Hurst exponent was found to steadily decrease with n (for example, $H=0.13$ and $H=0.19$ in the respective directions for $n=5$, see [9]).

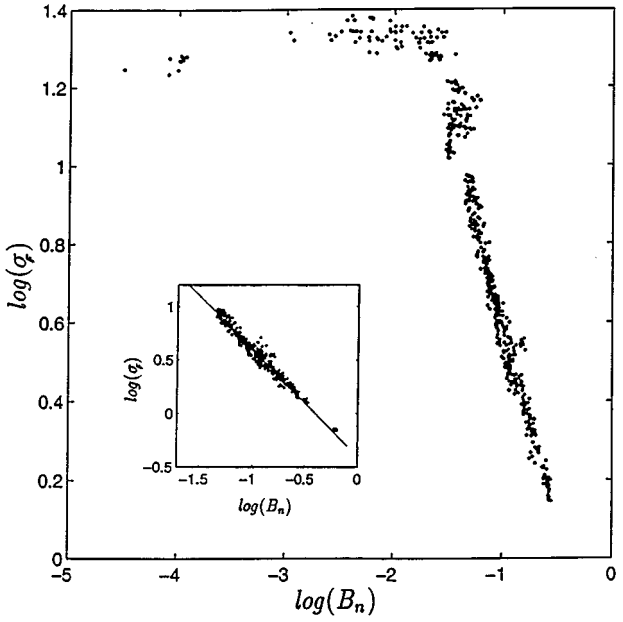

FIG. 8. Log-log plot of the front width σ_F vs B_n for different lattice sizes and for n in the range (0,3). The straight line in the inset has a slope of -1. Comparison with the theoretical slope $-[\nu/(\nu+1)]$, suggests that IPM is an IPG in a long-range correlated field ($\nu=\infty$).

The development of strong large-scale correlations at relatively small n is expected from the definition of the invasion rules. After the front has reached a steady-state mean velocity, the perturbations of two adjacent sites A and B would satisfy $\psi_B=\psi_A+\tau_{AB}^n$, if sites A and B are along the y direction, or $\psi_B=\psi_A+\tau_{AB}^n-\mathcal{L}_n^n$, if along the x direction (and where we assumed that the pairs of sites are the growth site and its next to be occupied site, respectively). Then, it is evident that the perturbations of adjacent sites are strongly correlated, and that this correlation diminishes with increasing n. However, this argument also shows that the correlation should be isotropic. We suspect that the anisotropy found in [9] is due to the early transient.

Using the above information we can establish a connection between IPM and IPG. The connection to IPG is demonstrated in Appendix B, where we show that after the early transient, IPM is an IPG with a Bond number given by

$$B_n=D_c\left[\frac{\overline{\frac{dV}{dx}}}{\sigma_{V_n}(x_F)}\right], \tag{18}$$

where the constant D_c solves an algebraic equation depending on the form of the scaling function g. The two keys to this relationship is the assumed scaling of V_n, Eq. (12), and the decay of the derivative of σ_{V_n} with distance, Eq. (15) (although for a 2D square lattice and a symmetric g the latter condition is not necessary, see Appendix B). Contrary to conventional IPG, however, the above Bond number is not constant but varies with x, as a result of the variation of σ_{V_n}. Equation (18) can be further approximated as

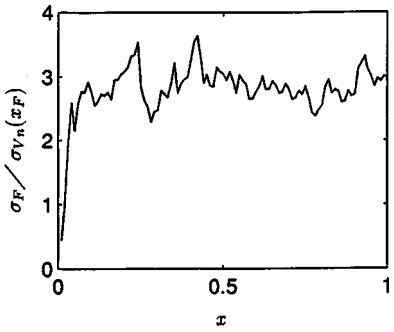

FIG. 9. Spatial variation of the ratio of the front width vs the standard deviation of V_1. The ratio stabilizes to a constant value after an early transient, consistent with the prediction of Eq. (21).

$$B_n\sim\frac{\mathcal{L}_n^n}{\sigma_{V_n}(x_F)}, \tag{19}$$

since C_n eventually approaches $\mathcal{L}_n^n$ (see below).

The identification of IPM with IPG allows us to express the scaling of the front width, σ_F, with the above-defined Bond number. Now, however, we must consider IPG in a correlated lattice with growing correlations, as suggested in Fig. 7. Despite this, the same arguments used for the conventional IPG scaling (17) apply here as well (see also [19]), except that ν should be the correlation length exponent corresponding to percolation in such a lattice. Percolation in long-range correlated lattices of the fBm type has been studied by Isichenko [20] who showed that for $H>0$ the correlation length exponent diverges, $\nu\to\infty$. For IPG in such lattices, therefore, substitution in Eq. (17) leads to the scaling

$$\sigma_F\sim B_n^{-1}. \tag{20}$$

The theoretical prediction (20) is tested in Fig. 8, which shows a plot of the front width, computed as in [1], vs the above-defined bond number. The data at relatively large B_n are fitted very well with a straight line of slope -1, as indeed predicted from Eq. (20). At smaller B_n (larger n), the slope decreases and eventually becomes zero, as the lateral lattice size interferes with the process (as in IPG) and the front width saturates.

Equation (20) also allows us to relate the standard deviation of V_n to that of the front. Substitution of Eq. (18) in Eq. (20) yields

$$\sigma_F\sim\sigma_{V_n}(x_F), \tag{21}$$

which suggests that the ratio of the front width to the standard deviation of V_n is constant. A plot of this ratio for a particular realization of IPM with $n=1$ is shown in Fig. 9. It is clear that after some early transients, the ratio fluctuates around a constant value, as predicted from Eq. (21). This behavior was also confirmed for other values of n, although the transient period increases with n. Equation (21) indicates that the variation of the front width with distance follows the same scaling as the standard deviation of V_n, which was conjectured in Eq. (15) to have a self-affine scaling. This leads to the result

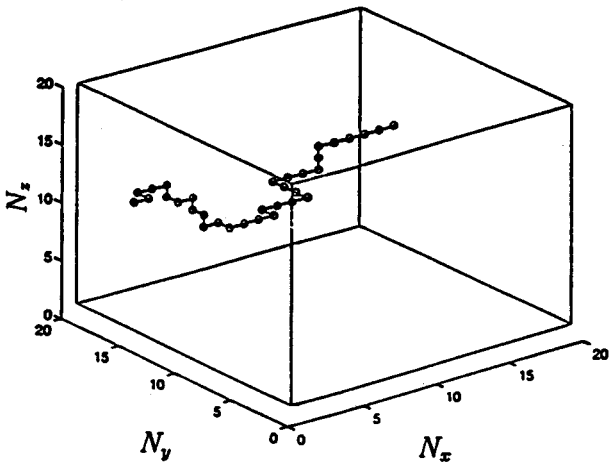

FIG. 10. The MTP for $n=1$ for a 3D cubic lattice $20\times20\times20$.

$$\sigma_F \sim L^{\xi_n} f_n\left(\frac{x}{L^{z_n}}\right), \tag{22}$$

where the function f has the same asymptotic scaling.

In summary, in this section we established a connection of IPM with IPG, with two important twists: that in IPM the probability gradient is generated dynamically during the process instead of being externally specified; and, at least for finite n, the process is one of gradient percolation in a *correlated* field. We note that identical findings also apply for the directed problem, hence a connection must exist between the DPRM problem and IPG in a correlated field. This connection is worth exploring further.

IV. GENERAL RESULTS

Using the preceding algorithm, various quantities of interest can be calculated. In particular, we consider the MTP, the minimum gradient, and the MTP tortuosity. A study of the distribution of thresholds can be found in [9]. All these results are for the nondirected case. Results for the directed problem will be reported in a future study.

Minimum threshold path

The MTP for $n=1$ is shown in Fig. 10 for invasion in a cubic lattice. Generalized MTPs for variable n were shown in Fig. 3. These vary from a straight line for $n=0$ to self-similar fractals for $n=|\infty|$. The increase in tortuosity as $|n|$ increases is due to the change of the invasion front from compact to self-affine to self-similar, as discussed above. For a finite n, therefore, and specifically for $n=1$, we expect that the MTP is a self-affine curve (in the more general definition of Feder [18], which also encompasses gradient percolation fronts) with a width that decreases as $|n|$ decreases. In particular, for sufficiently small $|n|$, the MTP coincides with the optimal path of DPRM. As $|n|\to\infty$, the MTP approaches a specific limiting curve. To understand its properties we first recall that for any n, the invading phase resides on self-avoiding dendritic branches emanating from the right boundary. These branches have the property that any two invaded sites on the same branch can be joined by only one self-avoiding path consisting of invaded sites, while invaded sites belonging to different branches cannot be joined by any such path (except by a path that passes from the origin). The MTP is part of the backbone of these branches, after dendritic fractions are suppressed. Figure 11 shows the backbones of the various branches at the breakthrough point for $n=1$ and $n=\infty$. In the first case (and also when $|n|$ is not large), many parallel-like branches coexist, and the MTP is the part of the particular branch that has reached the opposite side. However, in the percolation limit, $|n|=\infty$, a dominant branch develops. By definition, this branch, which is also the MTP at the $|n|=\infty$ limit, is the backbone of the cluster of a site-occupancy bond IP with bond trapping, obtained in the large $|n|$ limit. Therefore, in the general n case, the MTP is unrelated to a property of the percolation cluster. In particular, the MTP for $n=1$ is not a self-similar fractal, but instead it is a member of a general family of self-afine curves that includes as a limit (large $|n|$) the backbone of a site-bond percolation cluster. Because, contrary to regular site or bond percolation, this percolation process involves a *loopless* percolation cluster, the MTP in that limit is also a *loopless* fractal. It can be shown that the latter is a subset of the backbone of the invasion cluster in conventional bond percolation, but it does not coincide with the conventional chemical distance of percolation [9].

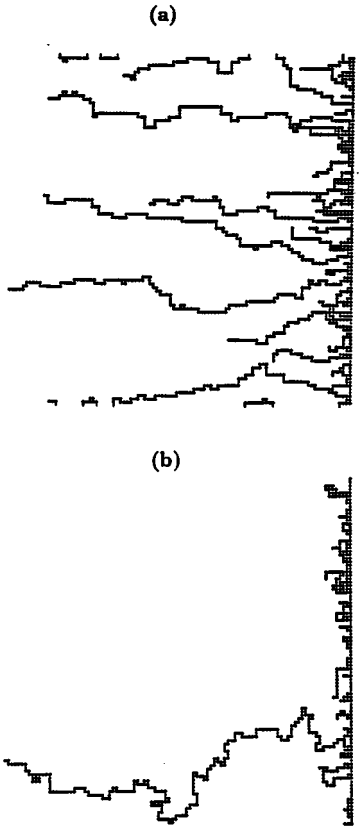

FIG. 11. The backbones of the dendritic branches, on which all invaded sites reside, originating from the right boundary for IPM with (a) $n=1$ and (b) $n=\infty$ (site-occupancy, bond-invasion percolation with bond trapping), from simulations in a 100×100 lattice. For $n=1$ the backbones appear self-affine and ''parallel'' to each other. Note the single dominant branch for $n=\infty$. The MTP for $n=\infty$ corresponds to the backbone of the loopless IP and it is a self-similar fractal. Periodic boundary conditions were used in the simulation.

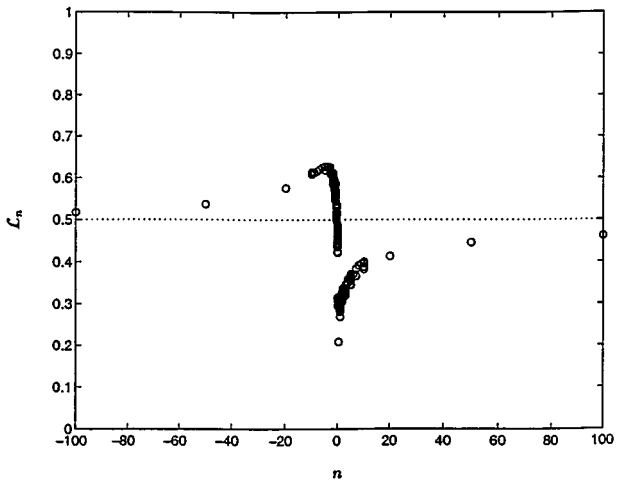

FIG. 12. The variation of the generalized minimum gradient $\mathcal{L}_n$ with n. Note the asymptotic approach to p_c and $1-p_c$ as n approaches ∞ and $-\infty$, respectively.

In a recent paper, pointed to us by one of the reviewers, Cieplak, Maritan, and Banavar [21] proposed a loopless IP similar to IPM for $n=\infty$. They reported that the backbone is a self-similar fractal with fractal dimension $D=1.22$ in 2D and $D=1.42$ in 3D. In agreement with our observations, they also found that the geometry of this backbone is not the same with that of the chemical distance on the percolation cluster.

Similar results are obtained for the optimal path of the DPRM problem in the large $|n|$ limit, which can be shown to be the loopless backbone of the corresponding directed IP cluster. The significance of the variation of the optimal path of the DPRM problem with n was commented in Sec. II.

Minimum gradient

Another quantity of significant interest is the generalized percolation threshold $\mathcal{L}_n$, which in the case $n=1$ reduces to the minimum gradient $|\nabla\Phi|_{\min}\equiv\mathcal{L}_1$. It was found that after some transients, $\mathcal{L}_1$ stabilizes to a mean value approximately equal to 0.305 ± 0.01. The corresponding value for 3D cubic lattices was found to be 0.196 ± 0.005. These compare well with the respective values of 0.29 and 0.17, reported by Sahimi [2]. The value of 0.22 found by Roux and Herrmann [1] in a square lattice tilted at 45° is also consistent with the above, if we make the obvious transformation $0.305/\sqrt{2}\approx0.22$, to reflect the difference in the definition of length L in the two problems. The latter results were also verified in [9] by additional simulations in a tilted 200×200 lattice, which gave the value of 0.2232.

The variation of the more general measure $\mathcal{L}_n$ with n is shown in Fig. 12 (including $n<0$). For positive n, this measure is a monotonically increasing function of n and approaches the limit $\mathcal{L}_\infty\rightarrow p_c=0.5$, as anticipated by Roux *et al.* [1]. Indeed, from definition, we have

$$\sum_i \tau_i^n=\tau_{\max}\left[1+\sum_{i\neq\max}\epsilon_i^n\right]\rightarrow\tau_{\max}^n, \tag{23}$$

where the notation is self-evident and we have taken $\epsilon_i=\tau_i/\tau_{\max}$. It follows that

$$\mathcal{L}_\infty=\min\lim_{n\rightarrow\infty}\frac{\tau_{\max}}{L^{1/n}}=\min\tau_{\max}\left(\frac{1}{L}\right)^0=\min\tau_{\max}=p_c, \tag{24}$$

where p_c is the threshold to a percolation process in which the front advances by invading the minimum threshold. A similar analysis holds for the opposite limit $n\rightarrow-\infty$, where the limit $\mathcal{L}_{-\infty}\rightarrow1-p_c$ was also verified. In view of the relation between the moments for general n and general PDFs, these results provide a qualitative picture of the dependence of the minimum sum of thresholds distributed from general PDFs, on the ratio of the standard deviation to the arithmetic mean.

We also note that $\mathcal{L}_n^n$ is related to the slope C_n of the spatial variation of the mean for the following reasons: The arithmetic mean V_n approaches the mean of V_n sampled over all front sites. However, the latter also approaches $\mathcal{L}_n^n$, because by construction, the maximum difference between any two values of V_n at the front is bounded by $\max\tau^n=1$. Hence, for a sufficiently large lattice or a sufficiently small n, all values at the front (including the minimum sum $\mathcal{L}_n^n$) eventually must grow at the same rate. This does not necessarily imply that the width of the front approaches a constant, however. Thus, we also expect the asymptotic relationship

$$\frac{d\overline{V_n}}{dx}\approx\mathcal{L}_n^n, \tag{25}$$

for all n.

Tortuosity of the MTP

A final quantity of interest is the tortuosity of the MTP. We expect the tortuosity to be constant for a self-affine curve and size dependent for a self-similar fractal. The variation of the tortuosity t_1, of the MTP with $n=1$ with lattice size was studied in [9], where it was found that although fluctuating at smaller sizes, it approaches a constant value at large sizes, the width of the fluctuations decreasing to zero. This adds support to our observation on the self-affinity of the MTP. From our simulations we found $t_1=1.31\pm0.01$ and 1.55 ± 0.02, for 2D square and 3D cubic lattices, respectively. These tortuosity data are new. The tortuosity of the generalized MTP was found to increase with n, however, reflecting the increased variance of the threshold distribution (see [9]).

Since the tortuosity is not a universal property, it will be affected by the particular shape of the threshold distribution. A simple, local, model for an arbitrary distribution of thresholds can be obtained as follows. We recall that the tortuosity of the MTP reflects the advantage incurred to the path in occasionally taking transverse steps that minimize the energy cost. Figure 13 shows schematically some of the infinitely many possibilities, for the advancement of the path in one increment in the direction, x. Denote by P_k the probability of the MTP taking a total of k steps in order to advance by a single increment in x,

$$P_k=\Pr[\tau_2+\tau_3+\cdots+\tau_{k+1}<\tau_1];\quad k=2,3,\ldots, \tag{26}$$

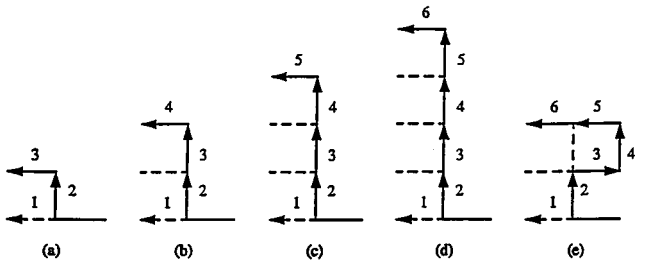

FIG. 13. Alternative pathways that can be taken by the MTP to advance by one step in the x direction (here from right-to-left). The possibilities of two steps (a), three steps (b), four steps (c), and five steps (d) and (e), are indicated. Note the backtracking (''overhang'') in (e).

where the values of τ are random thresholds from a given PDF. Then, the total path length l is equal to

$$l=L\left[1+\sum_{i=2,\infty} w_i(i-1)P_i\right], \tag{27}$$

where w_i is the number of different configurations corresponding to a given number of steps (for example, $w_5=2$ in Fig. 13). Given a PDF, the various probabilities above can be computed. In particular, for the case of a uniform PDF in (0,1), which is also the previous $n=1$ case, we can compute the probabilities of Eq. (26) to find [9]

$$P_k=\frac{1}{(k+1)!}. \tag{28}$$

For the tortuosity of the path requires that the weights w_i be computed. For the square lattice configuration of Fig. 13, $w_2=w_3=w_4=1$, but $w_5=2$, etc. Configurations of a larger number of steps have larger w_i, but substantially smaller probability. If, as an approximation, we take $w_i=1$ for all i, we obtain the result $t_1\approx 4-e=1.282$, which is reasonably close to the numerical value given above. The discrepancy is due to the assumption made. Inclusion of path multiplicity, which increases with k, will lead to an improved agreement. This simple model can be used to investigate the effect on the MTP tortuosity of more general PDFs [9], or to estimate the probability of an overhang in a path [such as depicted in Fig. 13(e), for example].

V. HIGHER-COST PATHS

In many applications, such as the flow of Bingham plastics and foams in porous media [2,3,22], the behavior following the onset of flow or displacement is of significant interest. In this context, the identification of paths of higher cost (energy) than the MTP is necessary. This problem also arises in the DPRM case, where patterns reminiscent of river deltas were found [5]. In this section, we use the IPM algorithm to identify these paths as the applied potential difference across the lattice increases. We note, again, that contrary to the DPRM problem, where all paths originate from a single point, here the paths can originate from many different points on the injection face.

When the applied potential gradient exceeds the minimum $|\nabla\Phi|>|\nabla\Phi|_{\min}$, additional bonds, not belonging to the MTP, can become open. The new paths that are formed are identified by the condition that the overall sum of thresholds on them exceeds the minimum potential difference but is smaller than or equal to the applied. We proceed by identifying the sequence of paths with progressively higher energy. Only the threshold across a bond is considered to contribute to the cost across an open bond (namely, there is no flow-induced potential drop, as would be for example the case in the flow of a Bingham plastic). The new paths can be completely new paths, unrelated to the MTP or other open paths, or they may share with them some of their bonds. In the latter case, an open path could act as a bridge between two already open paths, it may form a loop with one path, or it may connect one end of the lattice to a point of an already open path. The algorithm to find such paths must simultaneously identify the path and also determine its cost (the necessary potential gradient to make it open). It is described in the following. For simplicity, the discussion will be restricted to the $n=1$ case, the generalization to other values of n being straightforward.

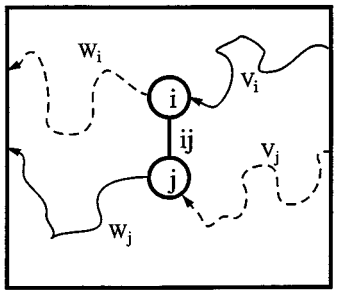

FIG. 14. The two alternative pathways (solid and dashed lines, respectively) that can lead to the opening of bond ij connecting adjacent sites i and j.

We recall that at the conclusion of IPM, a value V (where the subscript n was omitted) is assigned to every invaded site, that denotes the minimum overall threshold from the site to the right-hand side (RHS) boundary of the lattice. Consider, next, another IPM process, now from the left side, through which another function W, is assigned to each site, that denotes the minimum overall threshold from the site to the LHS boundary of the lattice. The minimum potential Φ_{ij} needed to open a bond between two adjacent lattice sites i and j (see Fig. 14) must be the minimum of the cost of the two alternative pathways, namely,

$$\Phi_{ij}=\min(V_i+\tau_{ij}+W_j, V_j+\tau_{ij}+W_i). \tag{29}$$

Hence, from a knowledge of the functions V and W at every site, the minimum potential to open a given bond, Φ_{ij}, can be computed.

Having assigned Φ, the algorithm proceeds sequentially from low to high energies by identifying the candidate bonds belonging to the next open path. Figure 15 shows the opening of the various paths as the potential difference increases. As expected, the first such path is the MTP. The successive opening of new paths is apparent in the model. These form correlated pathway regions (valleys), which are different than the paths of OP. The successive opening of pathways leads to ''flooded'' regions of increasing width analogous to the ''river deltas'' of the DPRM problem. Based on these

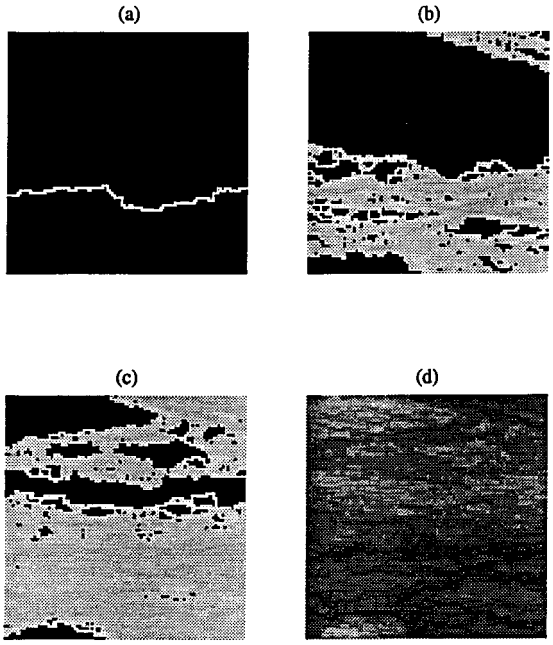

FIG. 15. Representation of the open paths as the applied potential increases at different stages: (a) MTP, (b) one-third, (c) two-thirds, and (d) three-thirds of all possible open paths, for a 100 $\times$100 lattice.

results, the fraction of bonds belonging to open paths vs the applied potential gradient can be computed. Figure 16 shows the results obtained. After the minimum gradient, the fraction of open bonds increases following an *S*-shape curve. The curve has percolationlike characteristics, in that there is a threshold $\mathcal{L}_1$, but it is not actually related to percolation, except in the limit of large n. In fact, the scaling of the curve (for $n=1$) near the threshold, was shown by Roux *et al.* [1] to be a power law with exponent equal to 2. The results of

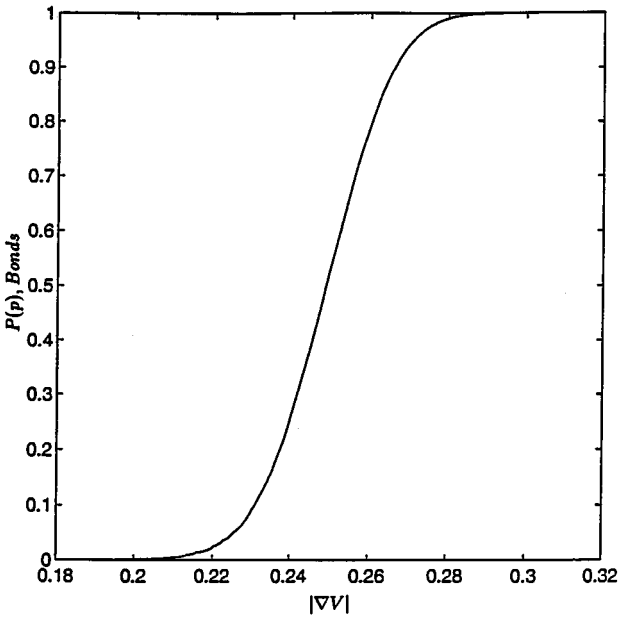

FIG. 16. The fraction of open bonds as a function of the applied gradient for $n=1$ from simulations in a 40$\times$40$\times$40 lattice.

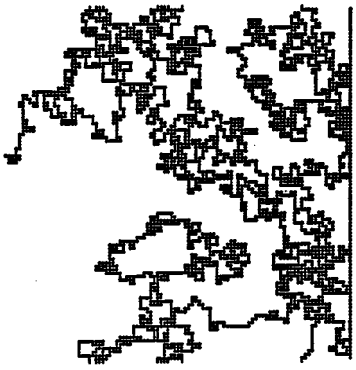

FIG. 17. Snapshot of unstable IPM with trapping, from simulations in a 100$\times$100 lattice. The pattern is a SAW constrained to occur on the LHS of the rightmost boundary.

Fig. 16 were used in [22] to model the fraction of flowing foam in porous media.

VI. UNSTABLE PROCESSES

In the above, we studied stable IPM. We can extend the study to ''unstable'' invasion processes, where the thresholds are viewed as gains, rather than penalties, and where instead of minimizing the cumulative threshold (penalty) we maximize the cumulative gain. Thus, the rule for the advance of the front would maximize, instead of minimizing, the measure S_n. The corresponding algorithm is trivially implemented. A typical snapshot of such processes from simulations in a 2D lattice is shown in Fig. 17, where a trapping rule was implemented. In the case of trapping, the invading phase consists of a singly connected self-similar thread of sites. Contrary to the previous case, the front is a self-similar fractal and was found to be identical for all n.

In the case of trapping, we can show that this path of maximum gain is a self-avoiding random walk (SAW) constrained to take place to the right of the invasion boundary. Indeed, by construction, the growth site is always the tip of the front, the site to be invaded next being the one of $Z-1$ neighbors (where Z is the coordination number of the lattice) with the largest value of $\tau^n_{F,F'}$. This process can be equivalently simulated by randomly advancing the tip to one of its neighboring unoccupied sites. The resulting path has the SAW properties. Because of the trapping rule, however, the path obtained is not the global maximum, which would obviously consist here of a path that covers the entire lattice (of dimension 2). Properties of SAW have been extensively discussed in previous references [23].

The difference in the invasion fronts as we switch from minimizing the penalty to maximizing the gain is similar to the change from IPG in a stabilizing gradient to IPG in a destabilizing gradient in percolation processes [24]. The rule of minimizing the cumulative penalty stabilizes the propagation of the front, in contrast to the rule of maximizing the cumulative gain, which creates a great degree of instability. A similarity can also be drawn between anti-diffusion-limited aggregation anti-DLA compact fronts and DLA fractal fronts [10], which characterize viscous stable and viscous unstable, respectively, displacements in porous media.

VII. CONCLUSIONS

Motivated by the problem of finding the path that minimizes the sum of thresholds in a lattice of elements with thresholds τ_i, randomly distributed in (0,1), we developed a class of invasion processes, in which the front advances by minimizing or maximizing the measure $S_n=\Sigma_i \tau_i^n$, where n is a real number. Because this rule assigns long-time memory to the invasion front, these processes belong to a new class of inversion percolation with memory (IPM). Depending on whether the rule minimizes or maximizes S_n, the invasion fronts are either stable and self-affine (case of minimum penalty) or unstable and fractal (case of maximum gain). The stable case was connected to IPG [7], but in a correlated lattice with self-affine correlations of the fBm type (positive Hurst exponent [18]), with IP [25] recovered in the limit $|n|=\infty$. In the unstable case, the IPM process was found to be a SAW, for any n. These processes also include as a special case the (simplest) problem of DPRM [5], by restricting the invasion to one direction. An important difference is that the IPM algorithm leads to optimal paths that can originate from any point along a curve.

The algorithm is well suited for the identification of minimum MTP that minimize the sum of τ_i^n across any two curves (as well as from any site to a given curve). For the corresponding DPRM problem, the MTP becomes the optimal path of DPRM, which for the case $n=1$, is known to be self-affine. In general, the MTP was shown to range from a straight line in the case of $n=0$ to a multifaceted curve at small n to a self-similar fractal in the large $|n|$ limit. The latter is the backbone of a mixed site-bond percolation cluster, and differs from the standard backbone of OP in that it does not contain reconnections (it is loopless). Its properties were recently studied in [21]. The MTP for $n=1$, corresponding to the classical problem, is not a self-similar fractal and does not coincide with the minimum path of OP. Instead, it is very closely related to the optimal path of DPRM and appears to be self-affine. The dependence of the MTP on n raises questions about the universality of the corresponding optimal path of the DPRM problem, when distributions with a large variance are considered. Various results on the MTP the minimum gradient and the path tortuosity were obtained. In particular, the algorithm allows the identification of paths of higher energy (cost), which generalize the ''river deltas'' of the DPRM problem.

ACKNOWLEDGMENTS

This work was supported in part by U.S. DOE Contract No. DE-FG22-93BC14899, the contribution of which is gratefully acknowledged.

APPENDIX A

Proving that $V_n(A)$ represents the minimum sum of thresholds from site A to the injection boundary, is equivalent to proving that the minimum threshold path from A to the injection boundary is the MTP determined algorithmically using the IPM process (path $\mathcal{L}$ in Fig. 18). First, we recall that through the IPM algorithm, *all* sites in the lattice can be invaded, and thus be assigned a unique value V_n. This can be accomplished by continuing the invasion process following breakthrough, and by also removing the trapping rule.

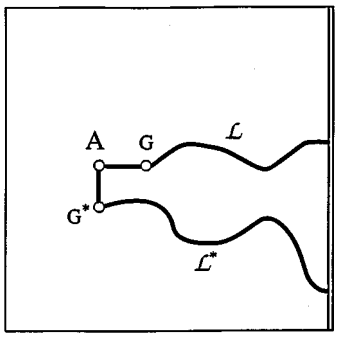

FIG. 18. Schematic of the various alternative minimum threshold paths from site A to the RHS boundary. Path $\mathcal{L}$ is the MTP of IPM, while $\mathcal{L}^*$ is the hypothetical alternative.

To prove our assertion, we use a *reduction in absurdio* argument: Assume that there exists another alternative path, denoted as $\mathcal{L}^*$ in Fig. 18, and consider the first site B on path $\mathcal{L}$ at which the two paths first diverge. Without loss in generality, we can take this site to be site A. (In the opposite case, we can apply the argument for site B. If the minimum threshold path from B is the MTP determined from the IPM algorithm, then, by extension, path $\mathcal{L}$ from A will also be the MTP). For future use, we consider the invasion stage when site A becomes invaded for the first time. In the notation of the text, at that time site A will be denoted as site G'. By construction, the value $V_n(A)$ assigned to it corresponds to the minimum value of $S_{n,FF'}=V_n(F)+\tau_{FF'}^n$, for every site F on the invasion front at that time. By the same token, $V_n(A)$ must also be larger than the value $V_n(I)$ assigned to all invaded sites I (including the front sites) prior to this time, since in the opposite case, site A would have been invaded at an earlier time. Hence, we have the inequalities

$$V_n(F)<V_n(A)\leqslant V_n(F)+\tau_{FF'}^n \tag{A1}$$

for all sites at the front. Furthermore, the second inequality also implies

$$V_n(A)<V_n(I') \tag{A2}$$

for all sites I' invaded following the invasion of site A. The corresponding MTP (path $\mathcal{L}$ in Fig. 18) connecting A to the RHS boundary is traced with the use of the IPM algorithm as discussed in the text. In particular, this path contains the bond AG, where G is the growth site for A.

Assume, now, that path $\mathcal{L}^*$ is the MTP. This implies that the sum of thresholds along this path is equal to a new value, $V_n^*(A)$, where

$$V_n^*(A)<V_n(A) \tag{A3}$$

and that site G^* on $\mathcal{L}^*$ adjacent to A has also assigned to it a value $V_n^*(G^*)$, such that

$$V_n^*(A)=V_n^*(G^*)+\tau_{G^*A}^n, \tag{A4}$$

where

$$V_n^*(G^*) < V_n(G^*). \tag{A5}$$

Inequality (A5) follows from the fact that in the reverse case, we would have $V_n^*(A) > V_n(A)$, due to (A1) and (A4), in case site G^* was a front site at the time site A was invaded, or due to (A2), in case G^* was invaded after site A. By comparing (A3) and (A5) it follows that to prove the existence of a path at A alternative to the MTP determined from the IPM algorithm, requires to prove the same for site G^*. By induction, therefore, the problem is reduced to proving the validity of inequality (A3) for the first ever site A invaded. But this is not possible, since for such a site, $V_n(A)$ represents by construction the minimum threshold adjacent to the injection face. It follows that inequalities (A5) and (A3) are not valid, thus, the MTP determined from the IPM algorithm is the path that minimizes the sum of thresholds, as claimed.

APPENDIX B

Consider bond invasion percolation in a field of V values (where we have omitted subscript n for simplicity), with the following PDF

$$f(V,x) = \frac{g(\theta)}{\sigma_V(x)}, \tag{B1}$$

where g is a function of the normalized variable $\theta = [V - \overline{V}(x)]/[\sigma_V(x)]$. Conventionally, in IP the front advances by penetrating the perimeter bond with the smallest value of V. Let the mean front position at a given stage of the process be x_F, and assume that the bond to be invaded next has the value V_M. Then, we can assign to any position x, a percolation probability fraction p

$$p(x) = \int_0^{V_M} f(V,x)\,dV, \tag{B2}$$

which, in view of (B1) can be simplified to

$$p(x) \approx G\left(\frac{V_M - \overline{V}(x)}{\sigma_V(x)}\right). \tag{B3}$$

Here we defined

$$G(\theta) = \int_{-\infty}^{\theta} g(\eta)\,d\eta \tag{B4}$$

and also assumed that x is sufficiently large for $\overline{V}(x)/\sigma_V(x) \gg 1$ [since at large x, σ_V grows slower than $V(x)$]. Now, (B3) also applies at the mean front position, where as is well known from the theory of gradient percolation [7], p is equal to the percolation threshold, p_c. Hence,

$$p_c = G\left(\frac{V_M - \overline{V}(x_F)}{\sigma_V(x_F)}\right). \tag{B5}$$

This is an algebraic equation with respect to the argument, the solution of which leads to an expression for V_M. By denoting its root by θ_c, we find

$$V_M = \sigma_V(x_F)\,\theta_c + \overline{V}(x_F). \tag{B6}$$

As an example, we may take a Gaussian distribution, for which the expressions corresponding to (B4) and (B5) read $G(\theta) = 1/2(1 + \mathrm{erf}\,\theta)$ and $p_c = 1/2[1 + \mathrm{erf}(V_M - \overline{V}(x_F))/\sigma_V(x_F)]$, respectively, and where θ_c is the root of

$$\tfrac{1}{2}(1 + \mathrm{erf}\ \theta_c) = p_c. \tag{B7}$$

In the latter case, we also have, $\theta_c = 0$, or $\theta_c = -0.48$ for a 2D square or a 3D cubic lattice, respectively. We note that the result $\theta_c = 0$ is also valid for all 2D square lattices with even g.

Now, we can substitute (B6) in (B3) and expand in a Taylor series around the mean front position x_F to obtain around the front

$$p = p_c - B(x - x_F) + O[(x - x_F)^2], \tag{B8}$$

where the Bond number B is equal to

$$B = G'(\theta_c)\left[\frac{\dfrac{d\overline{V}}{dx}}{\sigma_V(x_F)} + \theta_c \left.\frac{\dfrac{d\sigma_V}{dx}}{\sigma_V}\right|_F\right], \tag{B9}$$

which for a Gaussian, also reads

$$B = \frac{\exp(-\theta_c^2)}{\sqrt{\pi}}\left[\frac{\dfrac{d\overline{V}}{dx}}{\sigma_V(x_F)} + \theta_c \left.\frac{\dfrac{d\sigma_V}{dx}}{\sigma_V}\right|_F\right]. \tag{B10}$$

Thus, if we further assume that $(d\ \ln\sigma_V)/(dx)$ decreases with x to zero, the second term in the RHS inside the brackets becomes negligible at large x, hence

$$B \approx D_c\left[\frac{\dfrac{d\overline{V}}{dx}}{\sigma_V(x_F)}\right], \tag{B11}$$

where $D_c = G'(\theta_c)$. This relationship is exact for $\theta_c = 0.5$, for example for even PDF's in a square lattice.

[1] S. Roux, A. Hansen, and E. Guyon, J. Phys. **48**, 2125 (1987); S. Roux and H. J. Hermann, Europhys. Lett. **4**, 1227 (1987).

[2] M. Sahimi, AIChE J. **39**, 369 (1993); C. B. Shah, H. Kharabaf, and Y. C. Yortsos, in Fueling for a Clean and Safe Environment, edited by R. F. Meyer, Department of Energy, Report No. DE95000189 (1995) (unpublished).

[3] W. R. Rossen and C. K. Mamun, Phys. Rev. B **47**, 11815 (1993).

[4] B. Stauffer and A. Aharony, *Introduction to Percolation Theory*, 2nd ed. (Taylor and Francis, London, 1992).

[5] T. Halpin-Healy and Y.-C. Zhang, Phys. Rep. **254**, 215 (1995); A.-L. Barabasi and H. E. Stanley, *Fractal Concepts in Surface*

Growth (Cambridge University Press, Cambridge, England, 1995).

[6] M. Kardar, G. Parisi, and Y.-C. Zhang, Phys. Rev. Lett. **56**, 889 (1986).

[7] B. Sapoval, M. Rosso, and J. F. Gouyet, J. Phys. (Paris) Lett. **46**, L149 (1985); J. F. Gouyet, M. Rosso, and B. Sapoval, Phys. Rev. B **37**, 1832 (1988); J. P. Hulin, E. Clement, C. Baudet, J. F. Gouyet, and M. Rosso, Phys. Rev. Lett. **61**, 333 (1988).

[8] U. M. B. Marconi and Y.-C. Zhang, J. Stat. Phys. **61**, 885 (1990).

[9] H. Kharabaf, Ph.D. dissertation, University of Southern California, 1996.

[10] R. Lenormand, J. Phys. Condens. Matter **2**, SA79 (1990); M. Blunt, M. J. King, and H. Scher, Phys. Rev. A **46**, 7680 (1992).

[11] S. Roux and E. Guyon, J. Phys. A **22**, 3693 (1989); P. Meakin, J. Feder, V. Frette, and T. Jossang, Phys. Rev. A **46**, 3357 (1992); P. Meakin, A. Birovljev, V. Frette, J. Feder, and T. Jossang, Physica A **191**, 227 (1992).

[12] M. M. Dias and D. J. Wilkinson, J. Phys. A **19**, 3131 (1986); see also Y. C. Yortsos and M. Sharma, AIChE J. **32**, 46 (1986).

[13] H. J. Herrmann, D. C. Hong, and H. E. Stanley, J. Phys. A **17**, L261 (1984).

[14] M. Kardar and Y.-C. Zhang, Phys. Rev. Lett. **58**, 2087 (1987).

[15] C. S. Nolle, B. Koiller, N. Martys, and M. O. Robbins, Phys. Rev. Lett. **71**, 2074 (1993); Physica A **205**, 342 (1994).

[16] J. M. Kim, A. J. Bray, and M. A. Moore, Phys. Rev. A **44**, 2345 (1991).

[17] M. Chaouche, N. Rakotomalala, D. Salin, B. Xu, and Y. C. Yortsos, Phys. Rev. E **49**, 4133 (1994).

[18] J. Feder, *Fractals* (Plenum, New York, 1988).

[19] L. A. N. Amaral, A.-L. Barabasi, S. V. Buldyrev, S. T. Harrington, S. Havlin, R. Sadr-Lahijany, and H. E. Stanley, Phys. Rev. E **51**, 4655 (1995).

[20] M. B. Isichenko, Rev. Mod. Phys. **64**, 961 (1992).

[21] M. Cieplak, A. Maritan, and J. R. Banavar, Phys. Rev. Lett. **76**, 3754 (1996).

[22] H. Kharabaf and Y. C. Yortsos, Soc. Pet. Eng. J. (to be published).

[23] B. Nienhuis, Phys. Rev. Lett. **49**, 1062 (1982); P. Grassberger, J. Phys. A **26**, 1023 (1993).

[24] V. Frette, J. Feder, T. Jossang, and P. Meakin, Phys. Rev. Lett. **68**, 3164 (1992).

[25] D. Wilkinson and J. F. Willemsen, J. Phys. A **16**, 3365 (1983).